Magnetomechanical coupling and ferromagnetic resonance in magnetic nanoparticles

Hedyeh Keshtgar,[1] Simon Streib,[2] Akashdeep Kamra,[3] Yaroslav M. Blanter,[2] and Gerrit E. W. Bauer[2,4]
[1]*Institute for Advanced Studies in Basic Science, 45195 Zanjan, Iran*
[2]*Kavli Institute of NanoScience, Delft University of Technology, Lorentzweg 1, 2628 CJ Delft, The Netherlands*
[3]*Fachbereich Physik, Universität Konstanz, D-78457 Konstanz, Germany*
[4]*Institute for Materials Research and WPI-AIMR, Tohoku University, Sendai 980-8577, Japan*
(Received 5 October 2016; revised manuscript received 20 March 2017; published 27 April 2017)

We address the theory of the coupled lattice and magnetization dynamics of freely suspended single-domain nanoparticles. Magnetic anisotropy generates low-frequency satellite peaks in the microwave absorption spectrum and a blueshift of the ferromagnetic resonance (FMR) frequency. The low-frequency resonances are very sharp with maxima exceeding that of the FMR, because their magnetic and mechanical precessions are locked, thereby suppressing the effective Gilbert damping. Magnetic nanoparticles can operate as nearly ideal motors that convert electromagnetic into mechanical energy. The Barnett damping term is essential for obtaining physically meaningful results.

DOI: 10.1103/PhysRevB.95.134447

I. INTRODUCTION

Magnetic nanoparticles (nanomagnets) are of fundamental interest in physics by forming a link between the atomic and macroscopic world. Their practical importance stems from the tunability of their magnetic properties [1], which is employed in patterned media for high density magnetic data storage applications [2] as well as in biomedicine and biotechnology [3–6]. Superparamagnetic particles are used for diagnostics, stirring of liquids, and magnetic tweezers [7]. The heat generated by the magnetization dynamics under resonance conditions is employed for hyperthermia cancer treatment [8–10]. Molecular based magnets can cross the border from the classical into the quantum regime [11,12]. The magnetic properties of individual atomic clusters can be studied by molecular beam techniques [13–15].

Einstein, de Haas, and Barnett [16,17] established the equivalence of magnetic and mechanical angular momentum of electrons by demonstrating the coupling between magnetization and global rotations. Spin and lattice are also coupled by magnetic anisotropy, induced either by dipolar forces or crystalline fields. A quite different interaction channel is the magnetoelastic coupling between lattice waves (phonons) and spin waves (magnons) with finite wave vectors. This magnetoelastic coupling between the magnetic order and the underlying crystalline lattice has been explored half a century ago by Kittel [18] and Comstock [19,20]. The coupling between spin and lattice causes spin relaxation including Gilbert damping of the magnetization dynamics [21,22].

"Spin mechanics" of thin films and nanostructures encompasses many phenomena such as the actuation of the magnetization dynamics by ultrasound [23–25], the dynamics of ferromagnetic cantilevers [26–28], spin current-induced mechanical torques [22,29], and rotating magnetic nanostructures [30]. The Barnett effect by rotation has been observed experimentally by nuclear magnetic resonance [31]. The coupled dynamics of small magnetic spheres has been studied theoretically by Usov and Liubimov [32] and Rusconi and Romero-Isart [33] in classical and quantum mechanical regimes, respectively. A precessing single-domain ferromagnetic needle is a sensitive magnetometer [34], while a diamagnetically levitated nanomagnet can serve as a sensitive force and inertial sensor [35]. A stabilization of the quantum spin of molecular magnets by coupling to a cantilever has been predicted [36,37] and observed recently [38].

Here we formulate the dynamics of rigid and single-domain magnetic nanoparticles with emphasis on the effects of magnetic anisotropy and shape. We derive the equations of motion of the macrospin and macrolattice vectors that are coupled by magnetic anisotropy and Gilbert damping. We obtain the normal modes and microwave absorption spectra in terms of the linear response to ac magnetic fields. We demonstrate remarkable changes in the normal modes of motion that can be excited by microwaves. We predict microwave-activated nearly undamped mechanical precession. Anisotropic magnetic nanoparticles are therefore suitable for studies of nonlinearities, chaos, and macroscopic quantum effects.

In Sec. II we introduce the model of the nanomagnet and give an expression for its energy. In Sec. III we discuss Hamilton's equation of motion for the magnetization of a freely rotating particle, which is identical to the Landau-Lifshitz equation. We then derive the coupled equations of motion of magnetization and lattice in Sec. IV. Our results for the easy-axis and easy-plane configurations are presented in Secs. V and VI. We discuss and summarize our results in Secs. VII and VIII. In the Appendices A–D we present additional technical details and derivations.

II. MACROSPIN MODEL

We consider a small isolated nanomagnet that justifies the macrospin and macrolattice approximations, in which all internal motion is adiabatically decoupled from the macroscopic degrees of freedom, rendering the magnetoelastic coupling irrelevant. We focus on nonspherical nanoparticles with mass density $\rho(\boldsymbol{r})$ and tensor of inertia

$$\mathcal{I} = \int d^3r\, \rho(\mathbf{r})[(\mathbf{r}\cdot\mathbf{r})\hat{1} - \mathbf{r}\otimes\mathbf{r}], \tag{2.1}$$

where $\hat{1}$ is the 3×3 unit matrix. The mechanical properties of an arbitrarily shaped rigid particle is identical to that of an

ellipsoid with a surface that in a coordinate system defined along the symmetry axes (in which $\mathcal{I}$ is diagonal) reads

$$\left(\frac{x}{c}\right)^2+\left(\frac{y}{b}\right)^2+\left(\frac{z}{a}\right)^2=1, \tag{2.2}$$

where a,b,c are the shape parameters (principal radii). The volume is $V=4\pi abc/3$, total mass $Q=\rho V$, and principal moments of inertia $I_1=Q(a^2+b^2)/5$, $I_2=Q(a^2+c^2)/5, I_3=Q(b^2+c^2)/5$. We focus in the following on prolate ($a>b=c$) and oblate ($a<b=c$) spheroids, because this allows analytic solutions of the dynamics close to the minimum energy state.

We assume that the particle is smaller than the critical size $d_{\rm cr}\sim 36\sqrt{AK_A}/(\mu_0 M_s^2)$ for magnetic domain formation [39], where A is the exchange constant, K_A the anisotropy constant, M_s the saturation magnetization, and $\mu_0=4\pi\times 10^{-7}\,\mathrm{N\,A^{-2}}$ the vacuum permeability. For strong ferromagnets these parameters are typically in the range $A\in[5,30]\,\mathrm{pJ\,m^{-1}}$, $K_A\in[10,20000]\,\mathrm{kJ\,m^{-3}}$, $M_s\in[0.4,1.7]\,\mathrm{MA\,m^{-1}}$, leading to $d_{\rm cr}\in[1,500]$ nm [39]. For a spherical particle of radius R with sound velocity v, the lowest phonon mode frequency is approximately [40]

$$\frac{\omega_{\rm ph}}{2\pi}\approx\frac{v}{4R}=0.25\left(\frac{v/\left(10^3\,\frac{\rm m}{\rm s}\right)}{R/\mathrm{nm}}\right)\mathrm{THz}, \tag{2.3}$$

while the lowest magnon mode (for bulk dispersion relation $\hbar\omega_{\rm mag}=Dk^2$)

$$\frac{\omega_{\rm mag}}{2\pi}\approx\frac{\pi D}{8\hbar R^2}=0.6\left(\frac{D/(\mathrm{meV\,nm^2})}{R^2/\mathrm{nm^2}}\right)\mathrm{THz}, \tag{2.4}$$

where the spin wave stiffness $D=2g\mu_B A/M_s$ is typically of the order $\mathrm{meV\,nm^2}$ [39], e.g., $D=2.81\,\mathrm{meV\,nm^2}$ for iron [41]. We may disregard spin and lattice waves and the effects of their thermal fluctuations when the first excited modes are at sufficiently higher frequencies than that of the total motion (the latter is typically in the GHz range) and therefore adiabatically decoupled [33,40], i.e., the macrospin and macrolattice model is valid. Thermal fluctuations of the magnetization with respect to the lattice do not play an important role below the blocking temperature, $T_B\sim K_A V/(25k_B)$ [42], where k_B is the Boltzmann constant. For $k_BT\ll VM_s\mu_0H_0$, thermal fluctuations of the magnetization with respect to the static external magnetic field H_0 are suppressed.

Under the conditions stipulated above the classical dynamics (disregarding translations of the center of mass) is described in terms of the magnetization vector $\mathbf{M}=M_s\mathbf{m}$ (with $|\mathbf{m}|=1$) and the three Euler angles (θ,ϕ,ψ) of the crystal orientation direction in terms of the axis $\mathbf{n}(\theta,\phi)$ and a rotation angle ψ around it (see Appendix A for details). The total energy can be split up into several contributions,

$$E=E_T+E_Z+E_D+E_K. \tag{2.5}$$

$E_T=\frac{1}{2}\mathbf{\Omega}^{\rm T}\mathcal{I}\mathbf{\Omega}$ is the kinetic energy of the rotational motion of the nanomagnet in terms of the angular frequency vector $\mathbf{\Omega}$. $E_Z=-\mu_0 V\mathbf{M}\cdot\mathbf{H}_{\rm ext}$ is the Zeeman energy in a magnetic field $\mathbf{H}_{\rm ext}$. $E_D=\frac{1}{2}\mu_0 V\mathbf{M}^{\rm T}\mathcal{D}\mathbf{M}$ is the magnetostatic self-energy with particle shape-dependent demagnetization tensor $\mathcal{D}$. $E_K=K_1V(\mathbf{m}\times\mathbf{n})^2$ is the (uniaxial) magnetocrystalline anisotropy energy, assuming that the easy axis is along $\mathbf{n}$, and K_1 is the material-dependent anisotropy constant.

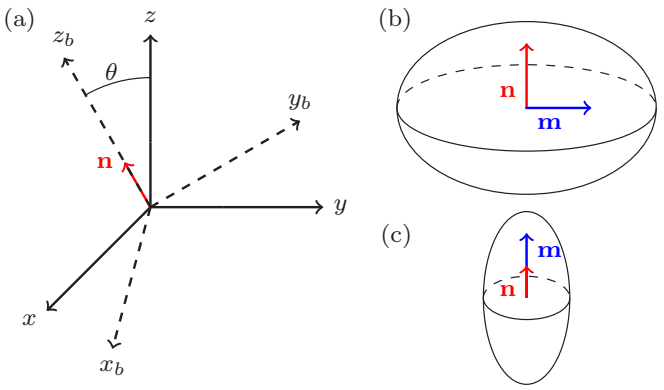

FIG. 1. (a) Laboratory frame (x, y, z) and (moving) body frame (x_b, y_b, z_b) of a nanomagnet with principal axis $\mathbf{n}$ along the z_b axis. The directions of $\mathbf{n}$ and magnetization $\mathbf{m}$ are shown for (b) oblate and (c) prolate spheroids with dipolar magnetic anisotropy.

We consider an inertial laboratory frame with origin at the center of mass and a moving frame with axes fixed in the body. The laboratory frame is spanned by basis vectors $\mathbf{e}_x,\mathbf{e}_y,\mathbf{e}_z$, and the body frame by basis vectors $\mathbf{e}_{x_b},\mathbf{e}_{y_b},\mathbf{e}_{z_b}$ (see Fig. 1). The body axes are taken to be the principal axes that diagonalize the tensor of inertia. For spheroids with $b=c$ the inertia and demagnetizing tensors in the body frame have the form

$$\mathcal{I}_b=\begin{pmatrix}I_\perp&0&0\\0&I_\perp&0\\0&0&I_3\end{pmatrix},\quad \mathcal{D}_b=\begin{pmatrix}D_\perp&0&0\\0&D_\perp&0\\0&0&D_3\end{pmatrix}, \tag{2.6}$$

with $I_\perp=Q(a^2+b^2)/5$ and $I_3=2Qb^2/5$; the elements $D_\perp$ and D_3 for magnetic spheroids are given in Ref. [43]. The particle shape enters the equations of motion via $I_\perp$, I_3, and the difference $D_3-D_\perp$; the latter reduces to $-1/2$ for a thin needle and 1 for a thin disk. When

$$E_\perp-E_\parallel=K_AV=K_1V-\tfrac{1}{2}\mu_0VM_s^2(D_3-D_\perp) \tag{2.7}$$

is larger than zero, the configuration $\mathbf{m}\parallel\mathbf{n}$ is stable ("easy axis"); otherwise $\mathbf{m}\perp\mathbf{n}$ ("easy plane"). The anisotropy constant K_A includes both magnetocrystalline and shape anisotropy.

III. LANDAU-LIFSHITZ EQUATION

For reference we rederive here the classical equation of motion of the magnetization. The magnetization of the particle at rest is related to the angular momentum $\mathbf{S}=-VM_s\mathbf{m}/\gamma$, where $\gamma=1.76\times10^{11}\,\mathrm{s^{-1}\,T^{-1}}$ is (minus) the gyromagnetic ratio of the electron. The Poisson bracket relations for angular momentum are

$$\{S_\alpha,S_\beta\}=\epsilon_{\alpha\beta\gamma}S_\gamma. \tag{3.1}$$

Hamilton's equation of motion reads

$$\frac{d}{dt}\mathbf{S}=\{\mathbf{S},\mathcal{H}\}, \tag{3.2}$$

where $\mathcal{H} \equiv E$ is the Hamiltonian. We consider a general model Hamiltonian of a single macrospin coupled to the macrolattice,

$$\mathcal{H} = \sum_{i,j,k\in\mathbb{N}_0} a_{ijk}(\mathbf{n},\mathbf{L}) S_x^i S_y^j S_z^k, \tag{3.3}$$

where the coefficients $a_{ijk}(\mathbf{n},\mathbf{L})$ may depend on the orientation $\mathbf{n}$ of the lattice and its mechanical angular momentum $\mathbf{L} = \mathcal{I}\Omega$. Since lattice and magnetization are different degrees of freedom, the Poisson brackets $\{\mathbf{n},\mathbf{S}\} = \{\mathbf{L},\mathbf{S}\} = 0$ and therefore $\{a_{ijk}(\mathbf{n},\mathbf{L}),\mathbf{S}\} = 0$. We derive in Appendix B

$$\{\mathbf{S},\mathcal{H}\} = \sum_{i,j,k\in\mathbb{N}_0} a_{ijk}(\mathbf{n},\mathbf{L}) \begin{pmatrix} i S_x^{i-1} S_y^j S_z^k \\ j S_x^i S_y^{j-1} S_z^k \\ k S_x^i S_y^j S_z^{k-1} \end{pmatrix} \times \mathbf{S}, \tag{3.4}$$

which is the Landau-Lifshitz equation [44],

$$\frac{d}{dt}\mathbf{S} = \nabla_{\mathbf{S}}\mathcal{H}|_{\mathbf{n},\mathbf{L}=\text{const.}} \times \mathbf{S}. \tag{3.5}$$

In accordance with Eq. (3.4), the gradient in Eq. (3.5) has to be evaluated for constant $\mathbf{n}$ and $\mathbf{L}$.

The rotational kinetic energy $E_T = \frac{1}{2}\mathbf{\Omega}^{\mathrm{T}}\mathcal{I}\mathbf{\Omega}$ does not contribute to this equation of motion directly since $\{\mathbf{S}, E_T\} = 0$. However, E_T is crucial when considering the energy of the nanomagnet under the constraint of conserved total angular momentum $\mathbf{J} = \mathbf{L} + \mathbf{S}$. Minimizing the energy of the nanomagnet under the constraint of constant $\mathbf{J}$ is equivalent to

$$\tilde{\mathbf{H}}_{\text{eff}} = -\frac{1}{\mu_0 V M_s}\nabla_{\mathbf{m}} E\Big|_{\mathbf{J}=\text{const.}} = 0, \tag{3.6}$$

where the rotational kinetic energy E_T contributes the Barnett field

$$\mathbf{H}_B = -\frac{1}{\mu_0 V M_s}\nabla_{\mathbf{m}} E_T\Big|_{\mathbf{J}=\text{const.}} = -\frac{\mathbf{\Omega}}{\gamma\mu_0}, \tag{3.7}$$

which gives rise to the Barnett effect (magnetization by rotation) [17]. Although the Barnett field appears here in the effective field $\tilde{\mathbf{H}}_{\text{eff}}$ when minimizing the energy, it is not part of the effective field $\mathbf{H}_{\text{eff}}$ of the Landau-Lifshitz equation,

$$\mathbf{H}_{\text{eff}} = -\frac{1}{\mu_0 V M_s}\nabla_{\mathbf{m}} E\Big|_{\mathbf{n},\mathbf{L}=\text{const.}}, \tag{3.8}$$

where $\mathbf{L}$ is kept constant instead of $\mathbf{J}$. In the Landau-Lifshitz-Gilbert equation in the laboratory frame the Barnett effect operates by modifying the Gilbert damping torque as shown below.

IV. EQUATIONS OF MOTION

We now derive the coupled equations of motion of the magnetization $\mathbf{m}$ and the Euler angles (ϕ,θ,ψ). The magnetization dynamics is described by the Landau-Lifshitz-Gilbert equation [21,44]

$$\dot{\mathbf{m}} = -\gamma\mu_0 \mathbf{m} \times \mathbf{H}_{\text{eff}} + \boldsymbol{\tau}_m^{(\alpha)}, \tag{4.1}$$

where the effective magnetic field Eq. (3.8) follows from the energy Eq. (2.5),

$$\mathbf{H}_{\text{eff}} = \mathbf{H}_{\text{ext}} + \mathbf{H}_D + \mathbf{H}_K, \tag{4.2}$$

and $\tau_m^{(\alpha)}$ is the (Gilbert) damping torque. The external magnetic field $\mathbf{H}_{\text{ext}}$ is the only source of angular momentum; all other torques acting on the total angular momentum $\mathbf{J} = \mathbf{L} - V M_s \mathbf{m}/\gamma$ cancel. From

$$\dot{\mathbf{J}} = \mu_0 V M_s \mathbf{m} \times \mathbf{H}_{\text{ext}}, \tag{4.3}$$

we obtain the mechanical torque as time derivative of the mechanical angular momentum, which leads to Newton's Law

$$\dot{\mathbf{L}} = \frac{V M_s}{\gamma}\dot{\mathbf{m}} + \mu_0 V M_s \mathbf{m} \times \mathbf{H}_{\text{ext}}. \tag{4.4}$$

The dissipation parameterized by the Gilbert constant [21] damps the relative motion of magnetization and lattice. In the body frame of the lattice [30]

$$\boldsymbol{\tau}_{m,b}^{(\alpha)} = \alpha \mathbf{m}_b \times \dot{\mathbf{m}}_b, \tag{4.5}$$

where the subscript b indicates vectors in the body frame. Transformed into the laboratory frame (see Appendix A)

$$\boldsymbol{\tau}_m^{(\alpha)} = \alpha[\mathbf{m} \times \dot{\mathbf{m}} + \mathbf{m} \times (\mathbf{m} \times \mathbf{\Omega})]. \tag{4.6}$$

This torque is an angular momentum current that flows from the magnet into the lattice [22]. Angular momentum is conserved, but the generated heat is assumed to ultimately be radiated away. In vacuum there is no direct dissipation of the rigid mechanical dynamics.

The Barnett field $\mu_0\mathbf{H}_B = -\mathbf{\Omega}/\gamma$ enters in the laboratory frame only in the damping term $\boldsymbol{\tau}_m^{(\alpha)}$. To leading order in α

$$\dot{\mathbf{m}} \approx -\gamma\mu_0 \mathbf{m} \times \mathbf{H}_{\text{eff}} - \alpha\gamma\mu_0 \mathbf{m} \times [\mathbf{m} \times (\mathbf{H}_{\text{eff}} + \mathbf{H}_B)] + \mathcal{O}(\alpha^2). \tag{4.7}$$

The contribution of $\mathbf{H}_B$ in the damping term causes the Barnett effect [17]. We find that this Barnett damping is very significant for the coupled dynamics even though no fast lattice rotation is enforced: Without Barnett damping the FMR absorption of the low-frequency modes described below would become negative.

V. EASY-AXIS CONFIGURATION

We first consider an easy-axis configuration ($\mathbf{m} \parallel \mathbf{n} \parallel \mathbf{e}_z$) in the presence of an external magnetic field with a large dc component H_0 along $\mathbf{e}_z$ and a small transverse ac component, $\mathbf{H}_{\text{ext}} = (h_x(t), \quad h_y(t), \quad H_0)^{\mathrm{T}}$, with $h_x(t) \propto h_y(t) \propto e^{i\omega t}$. Linearizing the equations of motion in terms of small transverse amplitudes, we can solve (4.1) and (4.4) analytically to obtain the linear response to $\mathbf{h}$ (see Appendix C for the derivation), i.e., the transverse magnetic susceptibility. Since we find $\dot{\Omega}_z = 0$, we disregard an initial net rotation by setting $\Omega_z = 0$. For small damping $\alpha \ll 1$, the normal modes are given by the positive solutions of the equations

$$\omega^3 \mp \omega^2\omega_0 - \omega\omega_c\omega_A \pm \omega_c\omega_A\omega_H = 0, \tag{5.1}$$

where $\omega_H = \gamma\mu_0 H_0$, $\omega_A = 2\gamma K_A/M_s$, $\omega_0 = \omega_H + \omega_A$, and $\omega_c = M_s V/(\gamma I_\perp)$ is the natural mechanical frequency governed by the spin angular momentum. Note that the equivalent negative solutions of Eq. (5.1) have the same absolute values as the positive solutions. We find that the FMR mode ω_0 is

blueshifted to $\omega_\parallel = \omega_0 + \delta\omega_\parallel$ with

$$\delta\omega_\parallel \approx \frac{\omega_A^2\omega_c}{\omega_0^2} > 0, \tag{5.2}$$

which is significant for small nanomagnets with large saturation magnetization and low mass density. It is a counterclockwise precession of **m** with **n** nearly at rest.

Two additional low-frequency modes emerge. For $\omega \ll \omega_0, \omega_A$ we may disregard the cubic terms in Eq. (5.1) and find

$$\omega_{l_{1,2}} \approx \sqrt{\left(\frac{\omega_c\omega_A}{2\omega_0}\right)^2 + \frac{\omega_H\omega_c\omega_A}{\omega_0}} \pm \frac{\omega_c\omega_A}{2\omega_0}. \tag{5.3}$$

At low frequencies, the magnetization can follow the lattice nearly adiabatically, so these modes correspond to clockwise and counterclockwise precessions of nearly parallel vectors **m** and **n**, but with a phase lag that generates the splitting. The frequency of the clockwise mode $\omega_{l_1} > \omega_{l_2}$ (see Fig. 3). Since magnetization and mass precess in unison, the effective Gilbert damping is expected to be strongly suppressed as observable in FMR absorption spectra as shown below.

The absorbed FMR power is (see Appendix D)

$$P = -\frac{\mu_0 V}{2}\omega \mathrm{Im}\left(\mathbf{h}_\perp^{*\mathrm{T}}\chi\mathbf{h}_\perp\right), \tag{5.4}$$

where $\mathbf{h}_\perp$ is the ac field normal to the static magnetic field $H_0\mathbf{e}_z$ and

$$\chi_{\alpha\beta} = \left.\frac{M_\alpha}{h_\beta}\right|_{\mathbf{h}_\perp=0} \tag{5.5}$$

is the transverse magnetic susceptibility tensor ($\alpha, \beta = x, y$). The diagonal ($\chi_{xx} = \chi_{yy}$) and the off-diagonal components ($\chi_{xy} = -\chi_{yx}$) both contribute to the absorption spectrum near the resonance frequencies, $|\mathrm{Im}\chi_{xx}| \approx |\mathrm{Re}\chi_{xy}|$. For $\alpha \ll 1$, we find that the sum rule

$$\int_0^\infty d\omega(-\omega\mathrm{Im}\chi_{xx}(\omega)) \approx \frac{\pi}{2}\omega_0\omega_M, \tag{5.6}$$

where $\omega_M = \gamma\mu_0 M_s$ does not depend on ω_c, meaning that the coupling does not generate oscillator strengths, only redistributes it. Close to a resonance

$$-\omega\mathrm{Im}\chi_{xx}(\omega) \sim F\frac{\eta^2}{(\omega-\omega_i)^2+\eta^2}, \tag{5.7}$$

with integral $\pi\eta F$. For the low-frequency modes the maximum $F \sim \frac{1}{2}\omega_M\omega_A^2/(\alpha\omega_H^2)$ with broadening $\eta \sim \frac{1}{2}\alpha\omega_c\omega_H^2/(\omega_A + \omega_H)^2$; for the FMR mode $F \sim \frac{1}{2}\omega_M/\alpha$ with $\eta \sim \alpha\omega_0$.

Let us consider an iron sphere with 2 nm diameter ($a = b = 1$ nm) under $\mu_0 H_0 = 0.65$ T or $\omega_H/(2\pi) = 18.2$ GHz. Its magnetization $\omega_M/(2\pi) = 60.33$ GHz, crystalline anisotropy $\omega_A/(2\pi) = 29.74$ GHz [45], and the magnetomechanical coupling $\omega_c/(2\pi) = 0.5(\mathrm{nm}/a)^2$ GHz. The blocking temperature is $T_B \sim 11(a/\mathrm{nm})^3$ K and $|E_Z|/(k_B T_B) \approx 30$, while the critical size for domain formation $d_{\mathrm{cr}} \sim 20$ nm [46,47]. We adopt a typical Gilbert damping constant $\alpha = 0.01$. The calculated FMR spectra close to the three resonances are shown in Fig. 2. Both low-frequency resonances are very sharp with a peak value up to 3.5 times larger than that of the high-frequency resonance, although the integrated intensity ratio is only

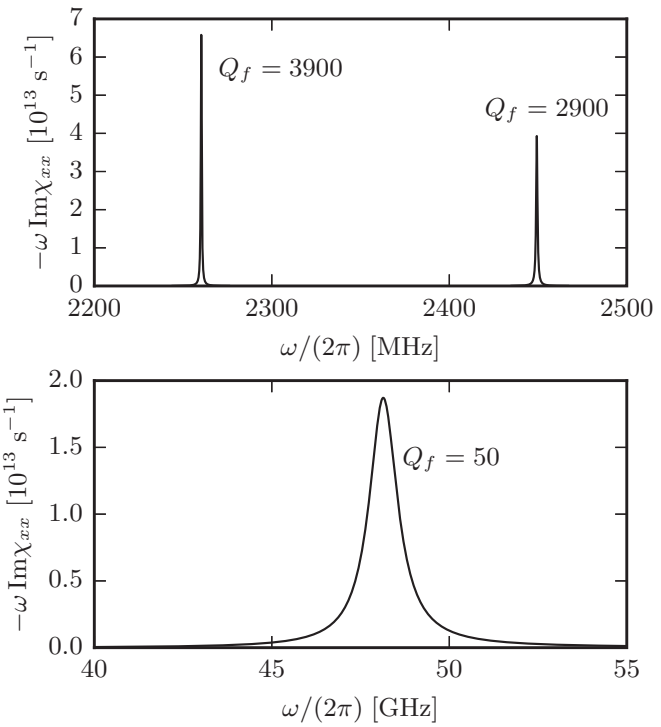

FIG. 2. Low- and high-frequency resonances in the FMR spectrum of an Fe nanosphere of 2 nm diameter in a static magnetic field of 0.65 T with Gilbert damping constant $\alpha = 0.01$; quality factor $Q_f = \omega/(2\eta)$.

0.2%. Long relaxation times of low-frequency modes that imply narrow resonances have been predicted for spherical nanomagnets [32]. The blueshift of the high-frequency resonance is $\delta\omega_\parallel/(2\pi) \approx 0.2(\mathrm{nm}/a)^2$ GHz. In Fig. 3 we plot the low-frequency modes ω_{l_1} and ω_{l_2} as a function of ω_H/ω_A. For $\omega_H/\omega_A \to 0$, $\omega_{l_1} \approx \omega_c$ and $\omega_{l_2} \to 0$. The low-frequency modes become degenerate in the limit $\omega_H/\omega_A \to \infty$.

In $\varepsilon - \mathrm{Fe_2O_3}$ [48] magnetization is reduced, resulting in $\omega_M/(2\pi) = 2.73$ GHz and $\omega_c/(2\pi) = 35(\mathrm{nm}/a)^2$ MHz. For the single-molecule magnet $\mathrm{TbPc_2}$ [38], we estimate $\omega_A/(2\pi) \sim 5$ THz [49], $\omega_M/(2\pi) \sim 10$ GHz, $\omega_c/(2\pi) \sim 100$ MHz [50], giving access to the strong-anisotropy regime with ultralow effective damping.

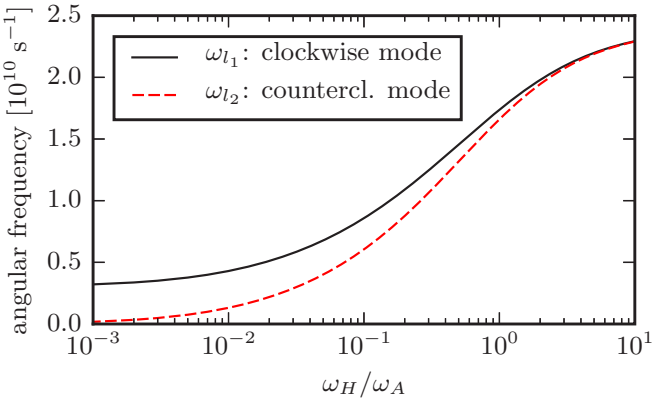

FIG. 3. Low-frequency magnetomechanical modes ω_{l_1} and ω_{l_2} of an Fe nanosphere of 2 nm diameter.

VI. EASY-PLANE CONFIGURATION

An easy-plane anisotropy aligns the equilibrium magnetization normal to the principal axis ($\mathbf{m} \perp \mathbf{n}$), which is typically caused by the shape anisotropy of pancake-like oblate spheroids corresponding to $\omega_A < 0$. We choose an external magnetic field with a static component in the plane $H_0\mathbf{e}_y$ and an ac field along x and z, while the equilibrium $\mathbf{n}$ points along $\mathbf{e}_z$ [see Fig. 1(b)]. For $\theta \ll 1$, $m_y \approx 1$, $n_z \approx 1$, we again obtain analytic solutions for $\mathbf{m}$ and $\mathbf{n}$ (see Appendix C). We find two singularities in the magnetic susceptibility tensor with frequencies (for $\alpha \ll 1$)

$$\omega_\perp \approx \omega_H \sqrt{1 - \frac{\omega_A}{\omega_H} - \frac{\omega_c \omega_A}{\omega_H^2}}, \tag{6.1}$$

$$\omega_l \approx \sqrt{\frac{\omega_H^2 \omega_c \omega_A}{\omega_A \omega_H - \omega_H^2 + \omega_c \omega_A}}. \tag{6.2}$$

Since n_x does not depend on time there is only one low-frequency mode ω_l, viz. an oscillation about the x axis of the nanomagnet. Linearization results in $\dot{L}_y \approx V M_s \dot{m}_y/\gamma \approx 0$ and implies $\dot{L}_y \approx I_\perp \ddot{n}_x \approx 0$. The high-frequency resonance $\omega_\perp$ is blueshifted by $\delta\omega_\perp \sim \omega_c$. As before, the lattice hardly moves in the high-frequency mode, while at low frequencies the magnetization is locked to the lattice.

In Fig. 4 we plot the FMR spectrum of an Fe nanodisk with shape parameters $a = 1$ nm and $b = 7.5$ nm under $\mu_0 H_0 = 0.25$ T or $\omega_H/(2\pi) = 7$ GHz. The characteristic frequencies are $\omega_c/(2\pi) = 17.2$ MHz and $\omega_A/(2\pi) = -14.4$ GHz. The blocking temperature with $|E_Z|/(k_B T_B) \approx 24$ is now about 300 K. Again, the low-frequency resonance is very sharp and relatively weak. The contribution of $\mathrm{Im}\chi_{xx}$ to the low-frequency resonance is by a factor of 600 smaller than the dominant $\mathrm{Im}\chi_{zz}$ and therefore not visible in the plot.

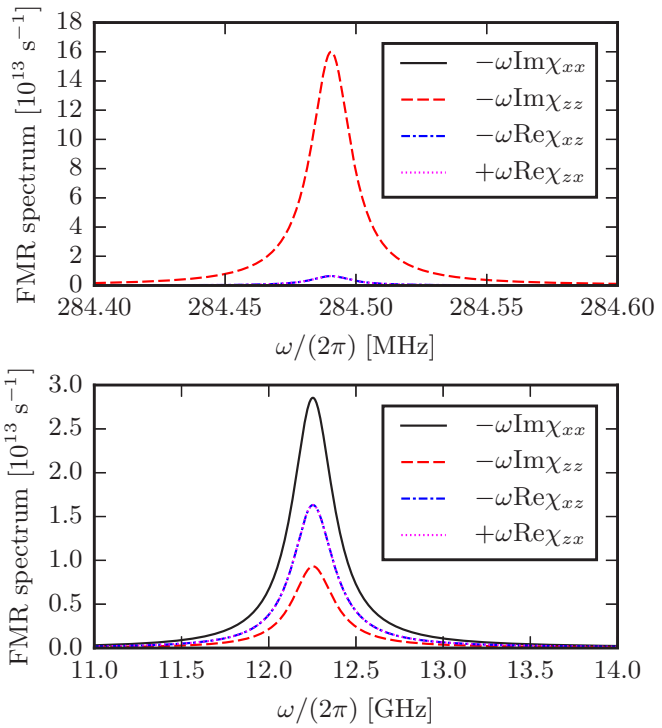

FIG. 4. FMR spectrum of an Fe disk with 15 nm diameter and 2 nm thickness in a static magnetic field of 0.25 T with Gilbert damping constant $\alpha = 0.01$.

VII. DISCUSSION

The examples discussed above safely fulfill all conditions for the validity of the theory either at reduced temperatures ($T < 11$ K, Fe sphere with 2 nm diameter) or even up to room temperature (2 nm × 15 nm Fe disk). The levitation of the particle can be achieved in cluster beams [13,15,51], in aerosols [52], or by confinement to a magnetic trap [33,35,53]. FMR experiments should preferably be carried out in a microwave cavity, e.g., a coplanar wave guide that can also serve as a trap [54].

Metal oxide nanoparticles, such as $\varepsilon - Fe_2O_3$ [48], have crystal anisotropies of the same order as that of pure iron but smaller magnetization, which reduces the magnetomechanical coupling strength, leading to similar results for somewhat smaller particles. The strongest anisotropies and couplings can be found in single-molecule magnets, e.g., $TbPc_2$ [49], but FMR experiments have to be carried out at low temperatures in order to suppress thermal fluctuations.

Our theory holds for isolated particles at sufficiently low temperatures and disregards quantum effects. According to the fluctuation-dissipation theorem a Gilbert damping is at finite temperatures associated with stochastic fields [55]. A full statistical treatment of the dynamics of magnetic nanoparticles at elevated temperatures, subject to microwaves, and weakly coupled to the environment is beyond the scope of the present paper. When not suspended in vacuum but in, e.g., a liquid, the mechanical motion encounters viscous damping and additional random torques acting on the lattice. Vice versa, the liquid in proximity of the particle will be stirred by its motion. These effects can be included in principle by an additional torque term in Eq. (4.4). The external torque will cause fluctuations in Ω_z and a temperature dependent broadening of the low-frequency resonances.

Microwave cavities loaded with thin films or spheres of the high-quality ferrimagnet yttrium iron garnet have received recent attention because of the relative ease with which the (ultra) strong coupling between magnons and photons can be achieved (for references and evidence for coherent magnon-phonon interaction, see Ref. [56]). The sharp low-frequency modes of free magnetic nanoparticles coupled to rf cavity modes at 10–100 MHz correspond to co-operativities that are limited only by the quality factor of the cavity. This appears to be a promising route to access nonlinear, chaotic, or quantum dynamical regimes. This technique would work also for magnets with large damping and could break the monopoly of yttrium iron garnet for quantum cavity magnonics. Materials with a large anisotropy are most attractive by the enhanced magnetization-lattice coupling.

VIII. SUMMARY

In conclusion, we discussed the effect of the magnetomechanical coupling on the dynamics of levitated single-domain spheroidal magnetic nanoparticles, e.g., in molecular cluster beams and aerosols. We predict a blueshift of the high-

frequency resonance and additional low-frequency satellites in FMR spectra that reflect particle shape and material parameters. In the low-frequency modes the nanomagnet precesses together with the magnetization with strongly reduced effective damping and thereby spectral broadening.

ACKNOWLEDGMENTS

This work is part of the research program of the Stichting voor Fundamenteel Onderzoek der Materie (FOM), which is financially supported by the Nederlandse Organisatie voor Wetenschappelijk Onderzoek (NWO) as well as JSPS KAKENHI Grants No. 25247056, No. 25220910, and No. 26103006. A.K. acknowledges financial support from the Alexander v. Humboldt foundation. H.K. would like to express her gratitude toward her late supervisor Malek Zareyan for the opportunity to collaborate with the TU Delft researchers. S.S. is grateful to Alejandro O. León for insightful discussions.

APPENDIX A: COORDINATE SYSTEMS AND TRANSFORMATIONS

We derive the coordinate transformation from the laboratory with basis vectors $\mathbf{e}_x$, $\mathbf{e}_y$, $\mathbf{e}_z$ to the body frame $\mathbf{e}_{x_b}$, $\mathbf{e}_{y_b}$, $\mathbf{e}_{z_b}$. The position of the particle is specified by the three Euler angles (ϕ,θ,ψ). These three angles are defined by the transformation matrix from the laboratory to the body frame ($\mathbf{r}_b = \mathcal{A}\mathbf{r}$),

$$\mathcal{A} = \begin{pmatrix} \cos\psi & \sin\psi & 0 \\ -\sin\psi & \cos\psi & 0 \\ 0 & 0 & 1 \end{pmatrix} \begin{pmatrix} 1 & 0 & 0 \\ 0 & \cos\theta & \sin\theta \\ 0 & -\sin\theta & \cos\theta \end{pmatrix} \times \begin{pmatrix} \cos\phi & \sin\phi & 0 \\ -\sin\phi & \cos\phi & 0 \\ 0 & 0 & 1 \end{pmatrix}. \tag{A1}$$

The main axis $\mathbf{n}$ of the particle is given by the local z_b axis in the body frame and can be directly obtained via the inverse transformation $\mathcal{A}^{\mathrm{T}}$,

$$\mathbf{n} = \begin{pmatrix} \sin\theta\sin\phi \\ -\sin\theta\cos\phi \\ \cos\theta \end{pmatrix}. \tag{A2}$$

The angular velocity vector of the rotating particle reads in the lab frame

$$\boldsymbol{\Omega} = \dot{\psi}\mathcal{A}^{\mathrm{T}}\begin{pmatrix} 0 \\ 0 \\ 1 \end{pmatrix} + \dot{\theta}\begin{pmatrix} \cos\phi & -\sin\phi & 0 \\ \sin\phi & \cos\phi & 0 \\ 0 & 0 & 1 \end{pmatrix}\begin{pmatrix} 1 \\ 0 \\ 0 \end{pmatrix} + \dot{\phi}\begin{pmatrix} 0 \\ 0 \\ 1 \end{pmatrix} = \begin{pmatrix} \dot{\theta}\cos\phi + \dot{\psi}\sin\theta\sin\phi \\ \dot{\theta}\sin\phi - \dot{\psi}\sin\theta\cos\phi \\ \dot{\phi} + \dot{\psi}\cos\theta \end{pmatrix}, \tag{A3}$$

and in the body frame,

$$\boldsymbol{\Omega}_b = \mathcal{A}\boldsymbol{\Omega} = \begin{pmatrix} \dot{\phi}\sin\theta\sin\psi + \dot{\theta}\cos\psi \\ \dot{\phi}\sin\theta\cos\psi - \dot{\theta}\sin\psi \\ \dot{\phi}\cos\theta + \dot{\psi} \end{pmatrix}. \tag{A4}$$

The mechanical angular momentum $\mathbf{L}$ and the principal axis $\mathbf{n}$ of the nanomagnet can be related by considering the mechanical angular momentum in the body frame

$$\mathbf{L}_b = \mathcal{I}_b\boldsymbol{\Omega}_b. \tag{A5}$$

Transforming (A5) to the laboratory frame and expanding for small angles θ,

$$L_x \approx I_\perp \frac{d}{dt}(\theta\cos\phi) \approx -I_\perp \dot{n}_y, \tag{A6a}$$

$$L_y \approx I_\perp \frac{d}{dt}(\theta\sin\phi) \approx I_\perp \dot{n}_x, \tag{A6b}$$

$$L_z \approx I_3(\dot{\phi} + \dot{\psi}) \approx I_3\Omega_z, \tag{A6c}$$

which is a valid approximation when $\Omega_z = \mathcal{O}(\theta)$. Furthermore, $n_z \approx 1$ and $\dot{n}_z \approx 0$ is consistent with $\theta \ll 1$.

The Gilbert damping is defined for the relative motion of the magnetization with respect to the lattice, i.e., in the rotating frame. The damping in the laboratory frame is obtained by the coordinate transformation

$$\boldsymbol{\tau}_m^{(\alpha)} = \mathcal{A}^{\mathrm{T}}\boldsymbol{\tau}_{m,b}^{(\alpha)} = \mathcal{A}^{\mathrm{T}}(\alpha\mathbf{m}_b \times \dot{\mathbf{m}}_b), \tag{A7}$$

where $\mathbf{m}_b = \mathcal{A}\mathbf{m}$. Expanding the time derivative

$$\boldsymbol{\tau}_m^{(\alpha)} = \alpha\mathbf{m} \times \dot{\mathbf{m}} + \alpha\mathbf{m} \times (\mathcal{A}^{\mathrm{T}}\dot{\mathcal{A}}\mathbf{m}). \tag{A8}$$

The angular frequency vector $\boldsymbol{\Omega}$ is defined by

$$\dot{\mathbf{r}} = \boldsymbol{\Omega} \times \mathbf{r}, \tag{A9}$$

where $\mathbf{r}$ is a point in the rotating body, i.e., $\dot{\mathbf{r}}_b = 0$, and

$$\dot{\mathbf{r}} = \dot{\mathcal{A}}^{\mathrm{T}}\mathbf{r}_b = \dot{\mathcal{A}}^{\mathrm{T}}A\mathbf{r}. \tag{A10}$$

Using $\frac{d}{dt}(\mathcal{A}^{\mathrm{T}}\mathcal{A}) = \mathcal{A}^{\mathrm{T}}\dot{\mathcal{A}} + \dot{\mathcal{A}}^{\mathrm{T}}A = 0$ and comparing Eqs. (A9) and (A10),

$$\mathcal{A}^{\mathrm{T}}\dot{\mathcal{A}}\mathbf{r} = \mathbf{r} \times \boldsymbol{\Omega}, \tag{A11}$$

and therefore

$$\boldsymbol{\tau}_m^{(\alpha)} = \alpha\mathbf{m} \times \dot{\mathbf{m}} + \alpha\mathbf{m} \times (\mathbf{m} \times \boldsymbol{\Omega}). \tag{A12}$$

APPENDIX B: POISSON BRACKET IN HAMILTON'S EQUATION

In the following, we show how to derive Hamilton's equation of motion (3.4). Using the linearity of the Poisson bracket together with the product rule

$$\{AB,C\} = A\{B,C\} + \{A,C\}B, \tag{B1}$$

and $\{a_{ijk}(\mathbf{n},\mathbf{L}),\mathbf{S}\} = 0$, we get

$$\{\mathbf{S},\mathcal{H}\} = \sum_{i,j,k\in\mathbb{N}_0} a_{ijk}(\mathbf{n},\mathbf{L})\{\mathbf{S},S_x^i S_y^j S_z^k\}. \tag{B2}$$

We only consider the x component, as the other components can be derived similarly. Using the product rule (B1), we may write

$$\{S_x,S_x^i S_y^j S_z^k\} = S_x^i\{S_x,S_y^j S_z^k\} = S_x^i S_y^j\{S_x,S_z^k\} + S_x^i S_z^k\{S_x,S_y^j\}. \tag{B3}$$

Next, we prove by induction that

$$\{S_x,S_z^k\} = -kS_yS_z^{k-1}, \tag{B4}$$

where the base case ($k = 0$)

$$\left\{S_x, S_z^0\right\} = 0 \tag{B5}$$

and the inductive step ($k \to k+1$)

$$\begin{aligned}\left\{S_x, S_z^{k+1}\right\} &= S_z\left\{S_x, S_z^k\right\} + S_z^k\{S_x, S_z\} \\ &= -(k+1)S_y S_z^k \end{aligned} \tag{B6}$$

complete the proof. Similarly, it follows

$$\left\{S_x, S_y^j\right\} = j S_y^{j-1} S_z. \tag{B7}$$

Summarizing

$$\begin{aligned}\left\{S_x, S_x^i S_y^j S_z^k\right\} = {} & j S_x^i S_y^{j-1} S_z^{k+1} \\ & - k S_x^i S_y^{j+1} S_z^{k-1}, \end{aligned} \tag{B8}$$

which gives with Eq. (B2) the x component of Eq. (3.4).

APPENDIX C: LINEARIZED EQUATIONS OF MOTION

1. Easy-axis configuration

In the easy-axis case ($\mathbf{m} \parallel \mathbf{n} \parallel \boldsymbol{e}_z$), the linearized equations of motion of the magnetization $\mathbf{m}$ and mechanical angular momentum $\mathbf{L}$ read

$$\dot{m}_x = -\omega_H m_y + \omega_M \frac{h_y}{M_s} - \omega_A(m_y - n_y) - \alpha(\dot{m}_y - \dot{n}_y), \tag{C1a}$$

$$\dot{m}_y = \omega_H m_x - \omega_M \frac{h_x}{M_s} + \omega_A(m_x - n_x) + \alpha(\dot{m}_x - \dot{n}_x), \tag{C1b}$$

$$\dot{m}_z = 0, \tag{C1c}$$

$$\dot{L}_x = -I_\perp \ddot{n}_y, \tag{C2a}$$

$$\dot{L}_y = I_\perp \ddot{n}_x, \tag{C2b}$$

$$\dot{L}_z = I_3 \dot{\Omega}_z = 0, \tag{C2c}$$

with

$$\ddot{n}_x = \omega_N^2(m_x - n_x) + \alpha\omega_c(\dot{m}_x - \dot{n}_x), \tag{C3a}$$

$$\ddot{n}_y = \omega_N^2(m_y - n_y) + \alpha\omega_c(\dot{m}_y - \dot{n}_y), \tag{C3b}$$

$$\ddot{n}_z = 0, \tag{C3c}$$

where $\omega_N^2 = \omega_c\omega_A$. Since $\dot{\Omega}_z = 0$ and with initial condition $\Omega_z = 0$, there is no net rotation Ω_z. Introducing the chiral modes,

$$m^\pm = m_x \pm i m_y, \quad n^\pm = n_x \pm i n_y, \quad h^\pm = h_x \pm i h_y, \tag{C4}$$

we can write the equations of motion in the compact form

$$\dot{m}^\pm = \pm i\left(\omega_0 m^\pm - \omega_M \frac{h^\pm}{M_s} - \omega_A n^\pm\right) \pm i\alpha(\dot{m}^\pm - \dot{n}^\pm), \tag{C5}$$

$$\ddot{n}^\pm = \omega_N^2(m^\pm - n^\pm) + \alpha\omega_c(\dot{m}^\pm - \dot{n}^\pm). \tag{C6}$$

For ac magnetic fields

$$h^\pm(t) = h_0^\pm e^{i\omega t}, \tag{C7}$$

we solve the equations of motion by the ansatz

$$m^\pm(t) = m_0^\pm e^{i\omega t}, \quad n^\pm(t) = n_0^\pm e^{i\omega t}. \tag{C8}$$

The observables correspond to the real part of the complex $\mathbf{m}$, $\mathbf{n}$, and $\mathbf{h}$. The susceptibilities are defined

$$m^\pm = \chi^\pm h^\pm / M_s, \quad n^\pm = \chi_n^\pm m^\pm, \tag{C9}$$

and read

$$\chi_n^\pm(\omega) = \frac{\omega_N^2 + i\alpha\omega\omega_c}{-\omega^2 + \omega_N^2 + i\alpha\omega\omega_c}, \tag{C10}$$

$$\begin{aligned}\chi^\pm(\omega) = {} & \mp\omega_M\left(-\omega^2 + \omega_N^2 + i\alpha\omega\omega_c\right) \\ & \times\left[(\omega \mp \omega_0 \mp i\alpha\omega)\left(-\omega^2 + \omega_N^2 + i\alpha\omega\omega_c\right)\right. \\ & \left. \pm \omega_c(\omega_A + i\alpha\omega)^2\right]^{-1}. \end{aligned} \tag{C11}$$

Close to a resonance of $\chi^\pm$ at ω_i the absorbed microwave power is determined by the contributions

$$-\frac{\omega}{2}\mathrm{Im}\chi^\pm(\omega) \sim F^\pm \frac{(\eta^\pm)^2}{(\omega - \omega_i)^2 + (\eta^\pm)^2}, \tag{C12}$$

with

$$\eta^\pm = \frac{\pm\alpha\omega_i\left(\omega_i^2 + \omega_c(\pm\omega_i - \omega_H)\right)}{3\omega_i^2 \mp 2\omega_i\omega_0 - \omega_c\omega_A}, \tag{C13}$$

$$F^\pm = \frac{\frac{1}{2}\omega_M\left(\omega_i^2 - \omega_c\omega_A\right)}{\alpha\left(\omega_i^2 + \omega_c(\pm\omega_i - \omega_H)\right)}. \tag{C14}$$

Note that for each resonance of χ^+ at ω_i there is a corresponding resonance of χ^- at $-\omega_i$.

The magnitudes of the x and y components of $\mathbf{n}$ are related to $\mathbf{m}$ via the susceptibility $\chi_n^\pm$ given in Eq. (C10). For high frequencies ω we find $\chi_n^\pm \approx 0$ and for low frequencies $\chi_n^\pm \approx 1$. Therefore, the main axis $\mathbf{n}$ is nearly static for the high-frequency mode, while for the low-frequency modes $\mathbf{n}$ stays approximately parallel to $\mathbf{m}$.

The susceptibility $\chi^\pm$ given in Eq. (C11) can be related to the usual magnetic susceptibilities ($\alpha, \beta = x, y$),

$$\chi_{\alpha\beta} = \left.\frac{M_\alpha}{h_\beta}\right|_{\mathbf{h}_\perp = 0}. \tag{C15}$$

Defining the symmetric and antisymmetric parts of the susceptibility $\chi^\pm$,

$$\chi^\pm = \chi_s \pm \chi_a. \tag{C16}$$

we find the relations

$$\chi_{xx} = \chi_{yy} = \chi_s, \tag{C17a}$$

$$\chi_{xy} = -\chi_{yx} = i\chi_a. \tag{C17b}$$

The magnetization dynamics in terms of the magnetic susceptibility reads

$$\mathrm{Re}\begin{pmatrix} m_x(t) \\ m_y(t) \end{pmatrix} = \mathrm{Re}\left[\begin{pmatrix} \chi_{xx} & \chi_{xy} \\ -\chi_{xy} & \chi_{xx} \end{pmatrix}\begin{pmatrix} h_x(t)/M_s \\ h_y(t)/M_s \end{pmatrix}\right], \tag{C18}$$

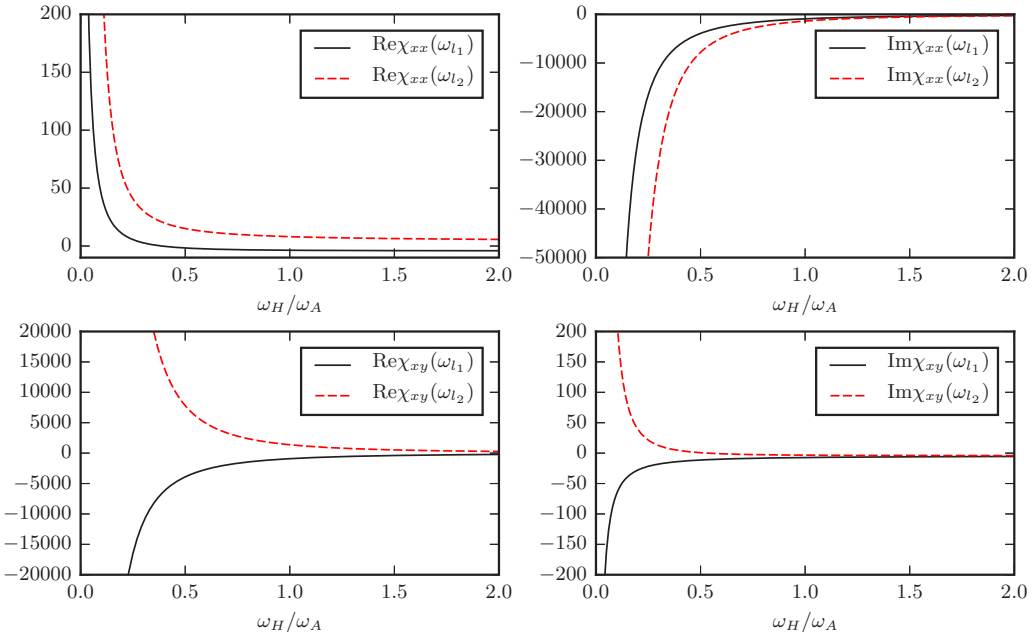

FIG. 5. Real and imaginary parts of the magnetic susceptibility tensor $\chi(\omega)$ of the low-frequency modes ω_{l_1} and ω_{l_2} for an Fe nanosphere of 2 nm diameter with Gilbert damping $\alpha = 0.01$.

where $\chi_{yy} = \chi_{xx}$ and $\chi_{yx} = -\chi_{xy}$. For linear polarization $h_x(t) = |h_x|e^{i\omega t}$ and $h_y(t) = 0$,

$$\mathrm{Re}\begin{pmatrix} m_x(t) \\ m_y(t) \end{pmatrix} = \frac{|h_x|}{M_s}\begin{pmatrix} \mathrm{Re}\chi_{xx}\cos(\omega t) - \mathrm{Im}\chi_{xx}\sin(\omega t) \\ -\mathrm{Re}\chi_{xy}\cos(\omega t) + \mathrm{Im}\chi_{xy}\sin(\omega t) \end{pmatrix}. \tag{C19}$$

According to Fig. 5, $|\mathrm{Re}\chi_{xx}|, |\mathrm{Im}\chi_{xy}| \ll |\mathrm{Re}\chi_{xy}| \approx |\mathrm{Im}\chi_{xx}|$, and $\mathrm{Im}\chi_{xx} < 0$ for both low-frequency modes ω_{l_1} and ω_{l_2}. The direction of the precession depends now on the sign of $\mathrm{Re}\chi_{xy}$, which is negative for ω_{l_1} and positive for ω_{l_2}. The mode ω_{l_1} is a clockwise precession,

$$\mathrm{Re}\begin{pmatrix} m_x(t) \\ m_y(t) \end{pmatrix} \propto \begin{pmatrix} \sin(\omega_{l_1} t) \\ \cos(\omega_{l_1} t) \end{pmatrix}, \tag{C20}$$

whereas the mode ω_{l_2} precesses counterclockwise:

$$\mathrm{Re}\begin{pmatrix} m_x(t) \\ m_y(t) \end{pmatrix} \propto \begin{pmatrix} \sin(\omega_{l_2} t) \\ -\cos(\omega_{l_2} t) \end{pmatrix}. \tag{C21}$$

Note that $\chi^-(\omega)$ has a low-frequency peak only at ω_{l_1} and $\chi^+(\omega)$ only at ω_{l_2} (for $\omega > 0$).

2. Easy-plane configuration

Here, we consider an equilibrium magnetization normal to the principal axis ($\mathbf{m} \perp \mathbf{n}$) due to the shape anisotropy of an oblate spheroid. Linearizing for small deviations from the equilibrium ($\theta \ll 1, m_y \approx 1, n_z \approx 1$), the equations of motion for the magnetization and mechanical angular momentum read

$$\dot{m}_x = \omega_H m_z - \omega_M \frac{h_z}{M_s} - \omega_A(m_z + n_y) + \alpha(\dot{m}_z + \dot{n}_y), \tag{C22a}$$

$$\dot{m}_y = 0, \tag{C22b}$$

$$\dot{m}_z = -\omega_H m_x + \omega_M \frac{h_x}{M_s} - \alpha\dot{m}_x - \alpha\Omega_z, \tag{C22c}$$

$$\dot{L}_x = -I_\perp \ddot{n}_y, \tag{C23a}$$

$$\dot{L}_y = I_\perp \ddot{n}_x, \tag{C23b}$$

$$\dot{L}_z = I_3\dot{\Omega}_z = \frac{VM_s}{\gamma}(-\alpha\dot{m}_x - \alpha\Omega_z), \tag{C23c}$$

with

$$\ddot{n}_x = 0, \tag{C24a}$$

$$\ddot{n}_y = \omega_N^2(m_z + n_y) - \alpha\omega_c(\dot{m}_z + \dot{n}_y), \tag{C24b}$$

$$\ddot{n}_z = 0. \tag{C24c}$$

In the presence of ac magnetic fields

$$h_x(t) = h_{x,0}e^{i\omega t}, \quad h_z(t) = h_{z,0}e^{i\omega t}, \tag{C25}$$

we use the ansatz

$$m_x(t) = m_{x,0}e^{i\omega t}, \quad m_z(t) = m_{z,0}e^{i\omega t}, \quad n_y(t) = n_{y,0}e^{i\omega t}. \tag{C26}$$

From Eq. (C23c)

$$\Omega_z = \frac{-\omega_I\omega\alpha m_x}{\omega - i\alpha\omega_I} \approx -\alpha\omega_I m_x, \tag{C27}$$

where $\omega_I = VM_s/(\gamma I_3)$ and provided $\alpha\omega_I$ is sufficiently smaller than all the other relevant frequencies. We approximate $\alpha\Omega_z = \mathcal{O}(\alpha^2) \approx 0$ in Eq. (C22c). Due to the reduced symmetry for $\mathbf{m} \perp \mathbf{n}$, we cannot simplify the equations of motion by introducing chiral modes but have to calculate the Cartesian components of the magnetic susceptibility tensor

χ as

$$\chi_{xx} = \omega_M\left[\omega^2(\omega_A - \omega_H) - i\alpha(\omega^3 - \omega\omega_c\omega_H) - \omega_H\omega_N^2\right]/\chi_d, \tag{C28a}$$

$$\chi_{zz} = -\omega_M(\omega_H + i\alpha\omega)\left(\omega^2 + \omega_N^2 - i\alpha\omega_c\omega\right)/\chi_d, \tag{C28b}$$

$$\chi_{xz} = i\omega\omega_M\left(\omega^2 + \omega_N^2 - i\alpha\omega_c\omega\right)/\chi_d, \tag{C28c}$$

$$\chi_{zx} = -\chi_{xz}, \tag{C28d}$$

where the denominator

$$\begin{aligned}\chi_d = {} & \omega^4(1+\alpha^2) + i\alpha\omega^3(\omega_A - \omega_c - 2\omega_H) \\ & + \omega^2\left(\omega_A\omega_H - \omega_H^2 + \omega_N^2 - \alpha^2\omega_c\omega_H\right) \\ & + i\alpha\omega\omega_H\left(\omega_c\omega_H - \omega_N^2\right) - \omega_H^2\omega_N^2.\end{aligned} \tag{C29}$$

The singularities in χ mark the two resonance frequencies. For small damping ($\alpha \ll 1$)

$$\begin{aligned}\omega_{1,2}^2 = {} & -\frac{1}{2}\left(\omega_A\omega_H - \omega_H^2 + \omega_N^2\right) \\ & \pm\frac{1}{2}\sqrt{\left(\omega_A\omega_H - \omega_H^2 + \omega_N^2\right)^2 + 4\omega_H^2\omega_N^2}.\end{aligned} \tag{C30}$$

From Eq. (C24b), we obtain the following relation between the magnetic and mechanical motion

$$n_y = \frac{-\omega_N^2 + i\alpha\omega_c\omega}{\omega^2 + \omega_N^2 - i\alpha\omega_c\omega} m_z. \tag{C31}$$

For high frequencies $n_y \approx 0$ and for low frequencies $n_y \approx -m_z$. This implies that for the high frequency mode $\omega_\perp = \omega_1$ we recover the bulk FMR, while in the low-frequency mode $\omega_l = \omega_2$ the magnetization is locked to the lattice.

APPENDIX D: FMR ABSORPTION

FMR absorption spectra are proportional to the energy dissipated in the magnet [25]. The energy density of the magnetic field is given by

$$w(t) = \tfrac{1}{2}\mathbf{H}(t)\cdot\mathbf{B}(t), \tag{D1}$$

where $\mathbf{B} = \mu_0\chi\mathbf{H}$. The absorbed microwave power by a magnet of volume V is

$$P(t) = V\dot{w}(t) = V\mathbf{H}(t)\cdot\dot{\mathbf{B}}(t). \tag{D2}$$

The average over one cycle $T = 2\pi/\omega$,

$$P \equiv \langle P(t)\rangle = \frac{1}{T}\int_0^T dt\, P(t), \tag{D3}$$

can be calculated using the identity

$$\langle \mathrm{Re}(\mathbf{A}e^{i\omega t})\cdot\mathrm{Re}(\mathbf{B}e^{i\omega t})\rangle = \tfrac{1}{2}\mathrm{Re}(\mathbf{A}^*\cdot\mathbf{B}). \tag{D4}$$

When a monochromatic ac component of the magnetic field $\mathbf{h}_\perp$ is normal to its dc component, the power reads

$$P = -\frac{\mu_0 V}{2}\omega\mathrm{Im}(\mathbf{h}_\perp^*\cdot\mathbf{M}_\perp), \tag{D5}$$

where $\mathbf{M}_\perp$ is the transverse magnetization. When the magnetization and static magnetic field are parallel to the principal axis of the particle, we can write

$$\begin{aligned}P = {} & -\frac{\mu_0 V}{2}\omega[(|h_x|^2 + |h_y|^2)\mathrm{Im}\chi_s(\omega) \\ & - 2\mathrm{Im}(h_x^* h_y)\mathrm{Im}\chi_a(\omega)],\end{aligned} \tag{D6}$$

where the symmetric and antisymmetric parts of the susceptibility $\chi^\pm$ Eq. (C11) as defined by Eq. (C16) obey the symmetry relations $\mathrm{Im}\chi_s(-\omega) = -\mathrm{Im}\chi_s(\omega)$ and $\mathrm{Im}\chi_a(-\omega) = \mathrm{Im}\chi_a(\omega)$. The term proportional to $\mathrm{Im}\chi_a$ can therefore be negative, depending on the signs of ω and $\mathrm{Im}(h_x^* h_y)$, whereas the term involving $\mathrm{Im}\chi_s$ (as well as the total absorbed power) is always positive.

When magnetization and static magnetic field are normal to the principal axis, both real and imaginary parts of the off-diagonal components of χ contribute to the absorbed power

$$\begin{aligned}P = {} & -\frac{\mu_0 V}{2}\omega[|h_x|^2\mathrm{Im}\chi_{xx}(\omega) + |h_z|^2\mathrm{Im}\chi_{zz}(\omega) \\ & + \mathrm{Im}(\chi_{xz}h_x^* h_z + \chi_{zx}h_x h_z^*)].\end{aligned} \tag{D7}$$

[1] A. G. Kolhatkar, A. C. Jamison, D. Litvinov, R. C. Willson, and T. R. Lee, Int. J. Mol. Sci. **14**, 15977 (2013).

[2] N. A. Frey and S. Sun, in *Inorganic Nanoparticles: Synthesis, Applications, and Perspectives*, edited by C. Altavilla and E. Ciliberto (CRC Press, Boca Raton, London, 2011), pp. 33–68.

[3] Q. A. Pankhurst, J. Connolly, S. K. Jones, and J. Dobson, J. Phys. D **36**, R167 (2003).

[4] P. Tartaj, M. del Puerto Morales, S. Veintemillas-Verdaguer, T. González-Carreño, and C. J. Serna, J. Phys. D **36**, R182 (2003).

[5] C. C. Berry and A. S. G. Curtis, J. Phys. D **36**, R198 (2003).

[6] A. van Reenen, A. M. de Jong, J. M. J. den Toonder, and M. W. J. Prins, Lab Chip **14**, 1966 (2014).

[7] M. M. van Oene, L. E. Dickinson, F. Pedaci, M. Köber, D. Dulin, J. Lipfert, and N. H. Dekker, Phys. Rev. Lett. **114**, 218301 (2015).

[8] I. Nándori and J. Rácz, Phys. Rev. E **86**, 061404 (2012).

[9] G. Vallejo-Fernandez, O. Whear, A. G. Roca, S. Hussain, J. Timmis, V. Patel, and K. O'Grady, J. Phys. D **46**, 312001 (2013).

[10] Z. Jánosfalvi, J. Hakl, and P. F. de Châtel, Adv. Cond. Mat. Phys. **2014**, 125454 (2014).

[11] O. Kahn, Acc. Chem. Res. **33**, 647 (2000).

[12] E. M. Chudnovsky, in *Molecular Magnets: Physics and Applications*, edited by J. Bartolomé, F. Luis, and F. J. Fernández (Springer, Berlin, Heidelberg, 2014), pp. 61–75.

[13] J. P. Bucher, D. C. Douglass, and L. A. Bloomfield, Phys. Rev. Lett. **66**, 3052 (1991).

[14] I. M. L. Billas, J. A. Becker, A. Châtelain, and W. A. de Heer, Phys. Rev. Lett. **71**, 4067 (1993).

[15] L. Ma, R. Moro, J. Bowlan, A. Kirilyuk, and W. A. de Heer, Phys. Rev. Lett. **113**, 157203 (2014).

[16] A. Einstein and W. J. de Haas, Proceedings KNAW **18 I**, 696 (1915).

[17] S. J. Barnett, Phys. Rev. **6**, 239 (1915).
[18] C. Kittel, Phys. Rev. **110**, 836 (1958).
[19] R. L. Comstock and B. A. Auld, J. Appl. Phys. **34**, 1461 (1963).
[20] R. L. Comstock, J. Appl. Phys. **34**, 1465 (1963).
[21] T. L. Gilbert, IEEE Trans. Magn. **40**, 3443 (2004).
[22] P. Mohanty, G. Zolfagharkhani, S. Kettemann, and P. Fulde, Phys. Rev. B **70**, 195301 (2004).
[23] K. Uchida, H. Adachi, T. An, T. Ota, M. Toda, B. Hillebrands, S. Maekawa, and E. Saitoh, Nat. Mater. **10**, 737 (2011).
[24] M. Weiler, H. Huebl, F. S. Goerg, F. D. Czeschka, R. Gross, and S. T. B. Goennenwein, Phys. Rev. Lett. **108**, 176601 (2012).
[25] D. Labanowski, A. Jung, and S. Salahuddin, Appl. Phys. Lett. **108**, 022905 (2016).
[26] A. A. Kovalev, G. E. W. Bauer, and A. Brataas, Appl. Phys. Lett. **83**, 1584 (2003).
[27] A. A. Kovalev, G. E. W. Bauer, and A. Brataas, Phys. Rev. Lett. **94**, 167201 (2005).
[28] A. A. Kovalev, G. E. W. Bauer, and A. Brataas, Jpn. J. Appl. Phys. **45**, 3878 (2006).
[29] A. G. Mal'shukov, C. S. Tang, C. S. Chu, and K. A. Chao, Phys. Rev. Lett. **95**, 107203 (2005).
[30] S. Bretzel, G. E. W. Bauer, Y. Tserkovnyak, and A. Brataas, Appl. Phys. Lett. **95** 122504 (2009).
[31] H. Chudo, M. Ono, K. Harii, M. Matsuo, J. Ieda, R. Haruki, S. Okayasu, S. Maekawa, H. Yasuoka, and E. Saitoh, Appl. Phys. Express **7**, 063004 (2014).
[32] N. Usov and B. Y. Liubimov, J. Magn. Magn. Mater. **385**, 339 (2015).
[33] C. C. Rusconi and O. Romero-Isart, Phys. Rev. B **93**, 054427 (2016).
[34] D. F. Jackson Kimball, A. O. Sushkov, and D. Budker, Phys. Rev. Lett. **116**, 190801 (2016).
[35] J. Prat-Camps, C. Teo, C. C. Rusconi, W. Wieczorek, and O. Romero-Isart, arXiv:1703.00221.
[36] A. A. Kovalev, L. X. Hayden, G. E. W. Bauer, and Y. Tserkovnyak, Phys. Rev. Lett. **106**, 147203 (2011).
[37] D. A. Garanin and E. M. Chudnovsky, Phys. Rev. X **1**, 011005 (2011).
[38] M. Ganzhorn, S. Klyatskaya, M. Ruben, and W. Wernsdorfer, Nat. Comm. **7**, 11443 (2016).
[39] J. Coey, *Magnetism and Magnetic Materials* (Cambridge University Press, Cambridge, UK, 2009).
[40] O. Romero-Isart, A. C. Pflanzer, M. L. Juan, R. Quidant, N. Kiesel, M. Aspelmeyer, and J. I. Cirac, Phys. Rev. A **83**, 013803 (2011).
[41] G. Shirane, V. J. Minkiewicz, and R. Nathans, J. Appl. Phys. **39**, 383 (1968).
[42] M. Knobel, W. C. Nunes, L. M. Socolovsky, E. De Biasi, J. M. Vargas, and J. C. Denardin, J. Nanosci. Nanotechnol. **8**, 2836 (2008).
[43] J. A. Osborn, Phys. Rev. **67**, 351 (1945).
[44] L. D. Landau and E. Lifshitz, Phys. Z. Sowjetunion **8**, 153 (1935).
[45] S.-J. Park, S. Kim, S. Lee, Z. G. Khim, K. Char, and T. Hyeon, J. Am. Chem. Soc. **122**, 8581 (2000).
[46] R. F. Butler and S. K. Banerjee, J. Geophys. Res. **80**, 252 (1975).
[47] A. Muxworthy and W. Williams, Geophys. J. Int. **202**, 578 (2015).
[48] S. Ohkoshi, A. Namai, K. Imoto, M. Yoshikiyo, W. Tarora, K. Nakagawa, M. Komine, Y. Miyamoto, T. Nasu, S. Oka, and H. Tokoro, Sci. Rep. **5**, 14414 (2015).
[49] N. Ishikawa, M. Sugita, T. Okubo, N. Tanaka, T. Iino, and Y. Kaizu, Inorg. Chem. **42**, 2440 (2003).
[50] M. Ganzhorn, S. Klyatskaya, M. Ruben, and W. Wernsdorfer, Nat. Nanotechnol. **8**, 165 (2013).
[51] I. M. Billas, A. Châtelain, and W. A. de Heer, Science **265**, 1682 (1994).
[52] C. Wang, S. K. Friedlander, and L. Mädler, China Particuol. **3**, 243 (2005).
[53] D. E. Pritchard, Phys. Rev. Lett. **51**, 1336 (1983).
[54] S. Bernon, H. Hattermann, D. Bothner, M. Knufinke, P. Weiss, F. Jessen, D. Cano, M. Kemmler, R. Kleiner, D. Koelle, and J. Fortágh, Nat. Commun. **4**, 2380 (2013).
[55] W. F. Brown, Phys. Rev. **130**, 1677 (1963).
[56] X. Zhang, C.-L. Zou, L. Jiang, and H. X. Tang, Sci. Adv. **2**, e1501286 (2016).